Hindawi Publishing Corporation
EURASIP Journal on Advances in Signal Processing
Volume 2009, Article ID 215409, 13 pages
doi:10.1155/2009/215409

Research Article

Nonlinear Analysis of the BOLD Signal

Zhenghui Hu,[1,2] Xiaohu Zhao,[3] Huafeng Liu,[1] and Pengcheng Shi[2,4]

[1] *Department of Optical Engineering, State Key Laboratory of Modern Optical Instrumentation, Zhejiang University, Hangzhou 310027, China*
[2] *B. Thomas Golisano College of Computing and Information Sciences, Rochester Institute of Technology, Rochester, NY 14623, USA*
[3] *Department of Radiology, Tongji Hospital of Tongji University, Shanghai 200065, China*
[4] *University of Rochester Medical Center, Rochester, NY 14642, USA*

Correspondence should be addressed to Pengcheng Shi, pengcheng.shi@rit.edu

Received 1 January 2009; Accepted 20 April 2009

Recommended by Don Johnson

The linearized filtering approach to the hemodynamic system is limited in capturing the inherent nonlinearities of physiological systems. The nonlinear estimation method therefore should be thought of as a natural way to access the nonlinear data assimilation problem. In this paper, we present a nonlinear filtering algorithm which is computationally expensive compared to the existing linearization filtering algorithms, for hemodynamic data assimilation, to address the deficiencies inherent to linearization. Simultaneous estimation of the physiological states and the system parameters have been demonstrated in a simulated and real data. The method provides more reasonable inference about the parameters of models for hemodynamic data assimilation.

Copyright © 2009 Zhenghui Hu et al. This is an open access article distributed under the Creative Commons Attribution License, which permits unrestricted use, distribution, and reproduction in any medium, provided the original work is properly cited.

1. Introduction

The primary goal of the fMRI study is to detect the underlying neural nature from the hemodynamics-induced signal intensity changes. The fMRI data analysis therefore aims to extract relevant spatio-temporal physiological information of the activation sites and the relationship between them. However, it is unfortunate that the hemodynamic signal is indirectly related to the neural activity, as it depends on a complex combination of changes in some physiological states, including cerebral blood flow (CBF), cerebral blood volume (CBV), and cerebral oxygen consumption rate ($CMRO_2$). Generally, the relationship between neural activity and the measurements of the BOLD signal may be modeled by the so-called hemodynamic responses function. This function describes the characteristic hemodynamic response to a brief neural event and thus characterizes the input-output behavior of a given voxel. An fMRI dataset typically consists of a series of time series associated with these intracerebral voxels. Then, for each voxel, the significance of the response to the stimulus is assessed by statistically analyzing the related fMRI time series based on the hemodynamic responses function; finally, a brain activation map can be constructed. Therefore, the knowledge of the hemodynamic responses function is essential for fMRI data analysis. Some of the better known functions include the Poisson function [1], the Gaussian function [2], the Gamma function [3, 4], inverse Logit function [5], and the linear combination of several functions [6, 7]. These functions are nothing more than empirical description of the phenomena, thus are exempt from the underlying phyiological bases of hemodynamic modulation. Those approaches based on these functions are also blind to the mechanisms that underlie physiological changes. For these reasons, most of current approach to fMRI analysis had been used primarily for activation detection, rather than for the exploration of the underlying physiology based on a detailed analysis of the BOLD response. However, it is important to have a quantitative understanding of those physiologic factors, such as changes in flow, oxygen extraction, blood volumes, and their combined effects, that are more directly related to the neural activity. These physiologically meaningful evaluations are needed to clarify the relationship between neural activation and experimental paradigm, and the significance of the observed transients in the BOLD signal [8].

Against this background, the Buxton-Friston (B-F) hemodynamic model has been developed as a comprehensive biophysical model of hemodynamic modulation. It combines the coupling mechanism of manifold physiological variables and has successfully simulated pronounced transients in the BOLD signal, including initial dips, overshoots, and a prolonged poststimulus undershoot. This model provides a possible platform to understand the dynamic changes of physiological variables during brain activation [9]. There have been many attempts at combining observational data with such a model in order to produce a reasonable inference about the physiological parameters and states of the system. Some modeled based optimisation approaches for estimating parameters from measured data were presented in [10–12]. A limitation of the above approaches is that they deal only with the measurement noise. Subsequently Riera et al. proposed a local linearization filter strategy that also considers physiological noise [13]. However, the hemodynamic response function typically possesses strong nonlinear characteristics that vary with the duration of hemodynamic modulation, making it questionable that such a linearized method addresses a strong nonlinear problem. The linearized Kalman filter approximation can lead to erroneous behavior of the linearized transform (Jacobian matrix) which substitutes nonlinear transformation at a given time. Thus, the linearized approximation method is only reliable when the time scale is discretized sufficiently small so that system is almost linear on the time scale, the error propagation can be well approximated by a linear function. Once the discretization violates this restriction, it can result in nonstable estimates. However, determining the validity of this assumption is extremely difficult because it depends on the transformation function, the current state, and the magnitude of the covariance. In addition, it is well known in the control community that the linearized filter approach is difficult to implement. It asks for a proper noise injection, which can overwhelm the inconsistent estimation error induced by the linearized transform, to produce positive definite covariance matrix. So, a nonlinear estimation algorithm should be considered as a natural choice for hemodynamic data assimilation studies. On the other hand, the nonlinear particle filter solution to the problem introduces some other difficulties while avoiding the deficiencies of linearization [14, 15]. In addition to computational expense, the accuracy of particle filter estimates degrades rapidly as sample point cloud is successively transformed [16]. While these filtering approaches above employed a Bayesian strategy, most recently, Friston et al. introduced two incremental estimation schemes, dynamic expectation maximisation (DEM) [17] and variational filtering [18], that address the assimilation problem as well.

In this paper, we describe a way of assimilating the fMRI time series that allow making inference about the underlying physiological states and the biophysical parameters generating observed fMRI signals. This corresponds to a nonlinear deconvolution of observed data using a hemodynamic state-space model based on stochastic differential equations. It allows one to deconvolve data, given known experimental inputs or perturbations. Our model can be regarded as a stochastic Dynamic Causal Model for a signal brain region, which allows for noise or random fluctuations on the underlying or hidden physiological states. Our deconvolution scheme uses an unscented Kalman filter and, computationally, is equivalent to the complexity of linear deconvolution schemes. In addition to inferring the hidden states, we also provide for inference on the parameters. This involves augmenting the state vector with the parameters and treating them as slowly varying states (as in variable parameter regression and related approaches). This scheme then is demonstrated on a simulated dataset and a real texture perception fMRI experiment. This paper is organized as follows. In the first section we introduce the heamodynamic model and motivate it to the state space formulation which forms the basis of hemodynamic data assimilation. Some physics notes on the model are presented in Section 3. In Section 4 we explain the details of the nonlinear filter implementation. Section 5 presents the results of a synthetic and a real data assimilation with the new method. Summary and conclusion are given in Section 6.

Notation 1. Throughout the paper, a continuous time differential equation and its discrete equation are denoted by lowercase (e.g., $\mathbf{h}$) and corresponding uppercase (e.g., $\mathbf{H}$) symbols, respectively. Notations such as $\boldsymbol{\beta}$ denote a vector or parameter set, while β_i means some entry of the vector.

2. Hemodynamics Model

The Buxton-Friston hemodynamic model describes the couples dynamics from synaptic activity to fMRI signals [10]. The process of equations describe the dynamics evolutions of the basic physiological state, including the cerebral blood flow f, the cerebral blood volume v, and the veins deoxyhemogolobin content q with the external input $u(t)$. It consists of three linked subsystems: (1) neural activity $u(t)$ to changes in flow f; (2) changes in flow f to changes in blood volume v; (3) changes in f, v, and oxygen extraction fraction to changes in deoxyhemoglobin q:

$$\begin{aligned}
\ddot{f} &= \epsilon u(t) - \frac{\dot{f}}{\tau_s} - \frac{f-1}{\tau_f}, \\
\dot{v} &= \frac{1}{\tau_0}\left(f - v^{1/\alpha}\right), \\
\dot{q} &= \frac{1}{\tau_0}\left(f\frac{1-(1-E_0)^{1/f}}{E_0} - v^{1/\alpha}\frac{q}{v}\right),
\end{aligned} \tag{1}$$

where $u(t)$ is the neuronal inputs; ϵ is neuronal efficacy; τ_s reflects signal decay; τ_f is the feedback autoregulation time constant; τ_0 is the transit time; α is the stiffness parameter; E_0 represent the resting oxygen extraction fraction. Their typical values and probability distributions are given in Table 1 [11]. All state variables are expressed in normalized form, relative to resting values. Equation (1) has a second-order time derivative, and we can write this system as a set of four first-order ODEs by introducing a new variable $s = \dot{f}$.

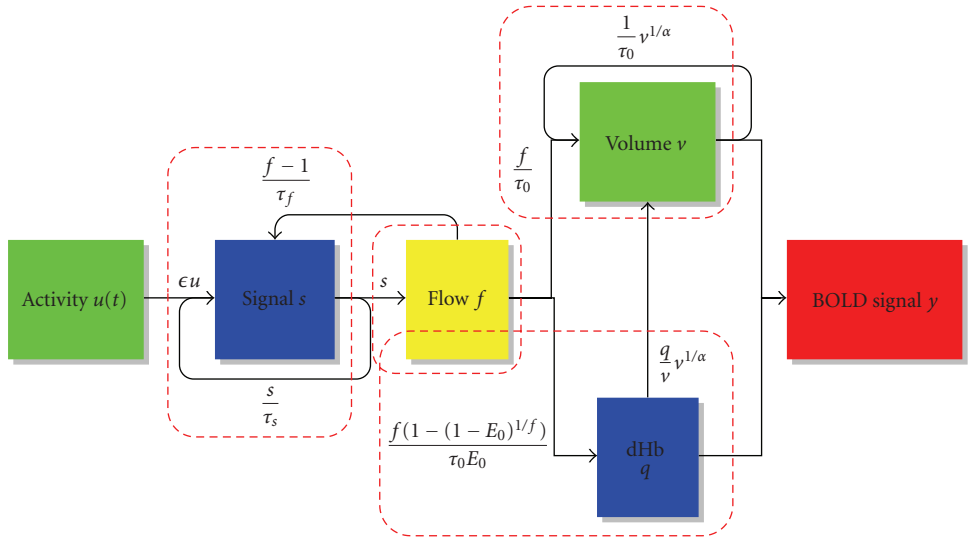

Figure 1: Schematic illustration of the hemodynamic model.

Table 1: Balloon model parameters and their probability distribution. $N(\mu, \sigma^2)$ denotes the normal distribution with mean μ and variance σ^2.

Notation	Definition	Distribution
ϵ	Neuronal efficacy	$\epsilon \sim N(0.54, 0.1^2)$
τ_s	Signal decay	$\tau_s \sim N(1.54, 0.25^2)$
τ_f	Autoregulation	$\tau_f \sim N(2.46, 0.25^2)$
τ_0	Transit time	$\tau_0 \sim N(0.98, 0.25^2)$
α	Stiffness parameter	$\alpha \sim N(0.33, 0.045^2)$
E_0	Resting oxygen extraction	$E_0 \sim N(0.34, 0.1^2)$

Furthermore, the output BOLD signal at the same voxel can be expressed as

$$y(t) = V_0\left(k_1(1-q) + k_2\left(1-\frac{q}{v}\right) + k_3(1-v)\right), \quad k_1 = 7E_0,\ k_2 = 2,\ k_3 = 2E_0 - 0.2, \tag{2}$$

appropriate for a 1.5 Tesla magnet [9]. V_0 is the resting blood volume fraction, where we imposed a physiological plausible value $V_0 = 0.03$ in the data assimilation process, as described in previous studies [10, 12]. The model architecture is summarised in Figure 1.

The stiffness parameter α shows a marginal influence to the system output variance in sensitivity analysis [19]. Therefore, it can be fixed within its physiological reasonable range ($\alpha = 0.33$, here) in system identification. There have been several enhancements of the original Balloon Model as well [20–22]. Such models have many degrees of freedom and can produce more desired behavior. For example, Zheng's model consists of 7 states and 13 parameters, twenty variates in all [20]. However, from a sensitivity analysis perspective, the original model is sufficient for sparse, noisy fMRI data assimilation [23].

Statistical models commonly can be explained as the fixed effects, which capture the underlying pattern, plus the error term. Thus, we rewrite (1), (2) as

$$\dot{\mathbf{x}} = f(\mathbf{x}, \boldsymbol{\beta}, \mathbf{u}, \mathbf{v}), \qquad v \sim N(0, \mathbf{R}_v), \tag{3}$$

$$\mathbf{y} = h(\mathbf{x}, \boldsymbol{\beta}, \mathbf{w}), \qquad w \sim N(0, \mathbf{R}_w), \tag{4}$$

where f and h are nonlinear equations, $\mathbf{x}(t) = [s, f, v, q]^T$ is the state of the system, $\boldsymbol{\beta} = \{\epsilon, \tau_s, \tau_f, \tau_0, E_0\}$ is system parameters, the neuronal inputs $\mathbf{u}$ represent system input, $\mathbf{v}$ is the noise process caused by disturbances and modeling errors, $\mathbf{y}$ is the observation vector, and $\mathbf{w}$ is measurement noise.

Equations (3) and (4) constitute a state-space representation of fMRI BOLD responses to given stimulation, and the goal of the data assimilation is then to estimate a set of hidden state variables $\mathbf{x}$ and parameter variables $\boldsymbol{\beta}$ based on the observation vector $\mathbf{y}$.

3. Dynamics in State Space

A state space ($\mathbf{x}(t) = [s, f, v, q]^T$) and a rule (1) for following the evolution of trajectories starting at various initial conditions constitute a dynamical system. It is interesting to build some intuitive understanding for its dynamics.

The fixed point of the system evolution can be found, by setting the four time derivatives equal 0,

$$\dot{\mathbf{x}}|_{x=x_0} = f(\mathbf{x}_0) = 0. \tag{5}$$

Thus, we have an equilibrium state:

$$x_0 = \begin{pmatrix} 0 \\ \epsilon\tau_f u_0 + 1 \\ \left(\epsilon\tau_f u_0 + 1\right)^{\alpha} \\ \dfrac{1-(1-E_0)^{1/(\epsilon\tau_f u_0+1)}}{E_0}\left(\epsilon\tau_f u_0 + 1\right)^{\alpha} \end{pmatrix}. \tag{6}$$

In particular, for the null input $u_0 = 0$, $\exists!\, \mathbf{x}_0 \in \mathbf{X} : \mathbf{x}_0 = [0,1,1,1]^T$. This value will be used as the initial value in subsequent system identification to accelerate the convergence of the algorithm.

The nature of the fixed point is determined by the characteristic values of the Jacobian matrix of partial derivatives evaluated at the fixed point. The Jacobian matrix for the set of equation is defined as

$$\mathbf{J} = \begin{pmatrix} -\dfrac{1}{\tau_s} & -\dfrac{1}{\tau_f} & 0 & 0 \\ 1 & 0 & 0 & 0 \\ 0 & \dfrac{1}{\tau_0} & -\dfrac{v^{1/\alpha-1}}{\alpha\tau_0} & 0 \\ 0 & \dfrac{1}{\tau_0}\left(\dfrac{1-(1-E_0)^{1/f}}{E_0} - \dfrac{(1-E_0)^{1/f}\ln(1-E_0)}{E_0 f}\right) & \dfrac{q}{\tau_0}\left(1-\dfrac{1}{\alpha}\right)v^{1/\alpha-2} & -\dfrac{v^{1/\alpha-1}}{\tau_0} \end{pmatrix}. \tag{7}$$

Its eigenvalues evaluated $\boldsymbol{\lambda}$ at the fixed point $\mathbf{x}_0$ are

$$\left\{ \frac{-1/\tau_s + \sqrt{1/\tau_s^2 - 4/\tau_f}}{2}, \frac{-1/\tau_s - \sqrt{1/\tau_s^2 - 4/\tau_f}}{2}, -\frac{\left(\epsilon\tau_f u_0 + 1\right)^{1-\alpha}}{\alpha\tau_0}, -\frac{\left(\epsilon\tau_f u_0 + 1\right)^{1-\alpha}}{\tau_0} \right\}. \tag{8}$$

Since the physiological parameters are always positive, these eigenvalues are either real and negative or have negative real parts ($\mathrm{Re}\,\lambda_i > 0$). These values dictate how the volumes contract along all directions of the coordinates of the phase space and mean that the volume will shrink to a point in time. Since the sum of the eigenvalues $\mathrm{Tr}(J) = \lambda_1 + \lambda_2 + \lambda_3 + \lambda_4 < 0$, it is a dissipative system. In the dissipative system, a trajectory starting from an initial condition in a phase space region stays near the fixed point for a time (transient) and then asymptotically approaches to an equilibrium state. The dissipative system evolves in time, and the trajectory in state space will head for the final equilibrium point. In other words, the hemodynamic main effect seems to be roughly a smoothing of the input and therefore has no long-term dynamic evolution behavior. Thus, our analyses concentrate mainly on the transient behavior associated with the start up of the system.

Furthermore, this is a nonautonomous system where the functions of the observables depend explicitly on time. We can augment the phase space by one dimension $\dot{t} = 1$ so that the system $\mathbf{x}(t) = [s, f, v, q]^T$ is autonomous, in where noncrossing trajectories occur. This allows us to specify time-dependent exogenous or experiment input in the context of an autonomous formulation.

Figures 2(a)–2(c) illustrate the behavior of the hemodynamic model to a 2-second stimulus for typical values of the seven parameters. The external stimulus was taken as the value 1 when the stimulus is ON and 0 when the stimulus is OFF (Figure 2(a)) [10, 12, 13, 19]. The resulting HRF with typical parameters values is shown in Figure 2(c). The stimulus results in a localized increase in neural activity, and the consumption of oxygen and the amount of dHb increase. Consequently, as compensation, an abrupt increase in blood flow results in a high blood volume and also causes some degree of attenuation in dHb content. All these predictions of the hemodynamic model concur with the known physiological effects in the BOLD signal. Figure 2(d) also shows a phase portrait for the short stimulus on the biophysical system.

4. Nonlinear Joint Estimation

We addressed this nonlinear state-space estimation ((3), (4)) using a square root unscented Kalman filter (SR-UKF) to maintain the nonlinearities presented in the hemodynamic model. UKF is a derivative-free alternative to the extended Kalman filter in the nonlinear case. It propagates the variables mean and covariance through the *unscented transformation* (UT) and possesses high accuracy and robustness for nonlinear model estimation [24, 25]. UT deterministically chooses a set of weighted *sigma points* so that the first two moments of these points match the prior distribution and propagates them through the actual nonlinear function. Then, the properties of the transformed set can be recalculated from these propagated points. It can capture the posterior mean and covariance accurately to the 3rd order (Taylor series expansion) for any nonlinearity [26].

The filtering algorithm consists essentially of two stages: prediction and update. The prediction stage uses the system model to predict the state posterior density (pdf) forward from one measurement time to the next:

$$\begin{aligned} \mathcal{X}_{k-1} &= [\hat{\mathbf{x}}_{k-1} \;\; \hat{\mathbf{x}}_{k-1} + \eta\mathbf{S}_{\mathbf{x}_{k-1}} \;\; \hat{\mathbf{x}}_{k-1} - \eta\mathbf{S}_{\mathbf{x}_{k-1}}], \\ \mathcal{X}_{k|k-1} &= F[\mathcal{X}_{k-1}, \mathbf{u}_{k-1}], \\ \hat{\mathbf{x}}_k^- &= \sum_{i=0}^{2L} W_i^{(m)} \mathcal{X}_{i,k|k-1}, \\ \mathbf{S}_{\mathbf{x}_k}^- &= \mathrm{qr}\left\{\left[\sqrt{W_i^{(c)}}\left(\mathcal{X}_{1:2L,k|k-1} - \hat{\mathbf{x}}_k^-\right); \mathbf{S}_v\right]\right\}, \\ \mathbf{S}_{\mathbf{x}_k}^- &= \mathrm{cholupdate}\left\{\mathbf{S}_k^-, \mathcal{X}_{0,k} - \hat{\mathbf{x}}_k^-, W_0^{(c)}\right\}. \end{aligned} \tag{9}$$

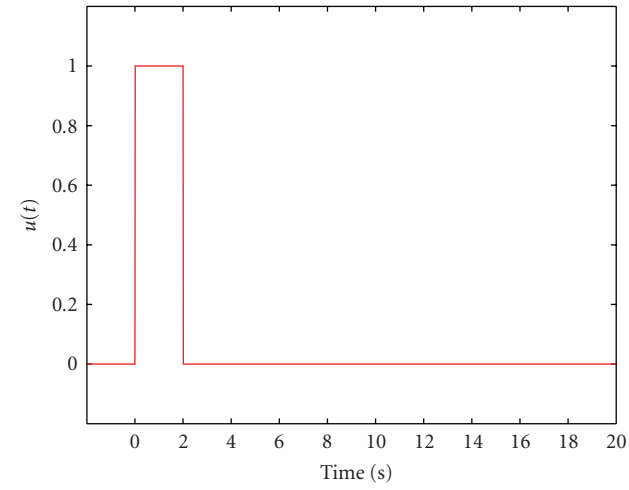

(a) $u(t)$

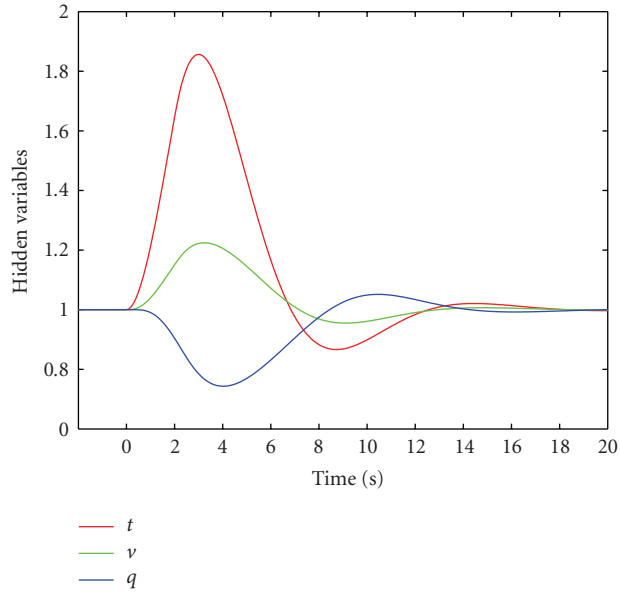

(b) Hidden state variables

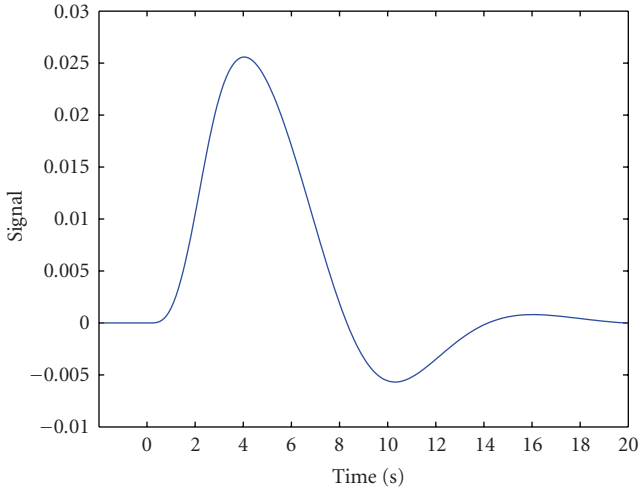

(c) Signal

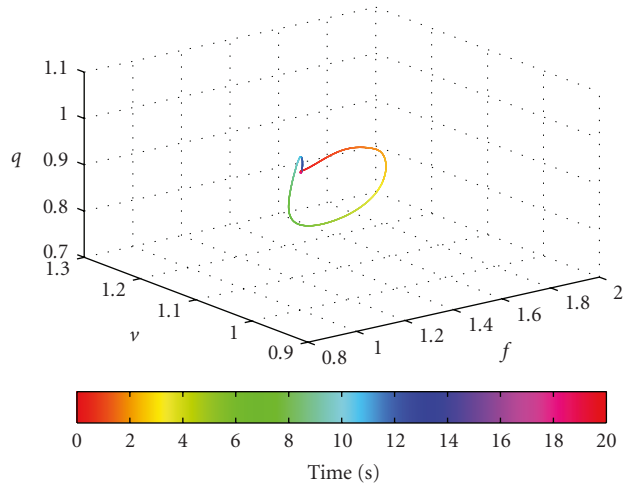

(d) Phase portrait

FIGURE 2: Simulation on an impulse input (1s) for typical parameter values. (a) impulse input; (b) the concomitant changes in blood flow (f, red), venous volume (v, green), and deoxyhemoglobin content (q, blue); (c) the corresponding BOLD response; (d) phase portrait for a three dimensional (f, q, v) phase space. $u(t)$ take the value 1 when the stimulus is ON and 0 when the stimulus is OFF.

The update operation then uses the latest measurement to modify the prediction pdf:

$$
\begin{aligned}
\mathcal{Y}_{k|k-1} &= \mathbf{H}\left[\mathcal{X}_{k|k-1}\right], \\
\hat{\mathbf{y}}_k^- &= \sum_{i=0}^{2L} W_i^{(m)} \mathcal{Y}_{i,k|k-1}, \\
\mathbf{S}_{\tilde{\mathbf{y}}_k} &= \mathrm{qr}\left\{\left[\sqrt{W_i^{(c)}}\left(\mathcal{Y}_{1:2L,k|k-1} - \hat{\mathbf{y}}_k^-\right); \mathbf{S}_w\right]\right\}, \\
\mathbf{S}_{\tilde{\mathbf{y}}_k}^- &= \mathrm{cholupdate}\left\{\mathbf{S}_{\tilde{\mathbf{y}}_k}, \mathcal{X}_{0,k} - \hat{\mathbf{y}}_k^-, W_0^{(c)}\right\}, \\
\mathbf{P}_{\mathbf{x}_k\mathbf{y}_k} &= \sum_{i=0}^{2L} W_i^{(c)}\left[\mathcal{X}_{i,k|k-1} - \hat{\mathbf{x}}_k^-\right]\left[\mathcal{Y}_{i,k|k-1} - \hat{\mathbf{y}}_k^-\right]^T, \\
\mathcal{K}_k &= \frac{\mathbf{P}_{\mathbf{x}_k\mathbf{y}_k}/\mathbf{S}_{\tilde{\mathbf{y}}_k}^T}{\mathbf{S}_{\tilde{\mathbf{y}}_k}}, \\
\hat{\mathbf{x}}_k &= \hat{\mathbf{x}}_k^- + \mathcal{K}_k\left(\mathbf{y}_k - \hat{\mathbf{y}}_k^-\right), \\
\mathbf{U} &= \mathcal{K}_k\mathbf{S}_{\tilde{\mathbf{y}}_k} \\
\mathbf{S}_{\mathbf{x}_k} &= \mathrm{cholupdate}\left\{\mathbf{S}_{\mathbf{x}_k}^-, \mathbf{U}, -1\right\},
\end{aligned}
\tag{10}
$$

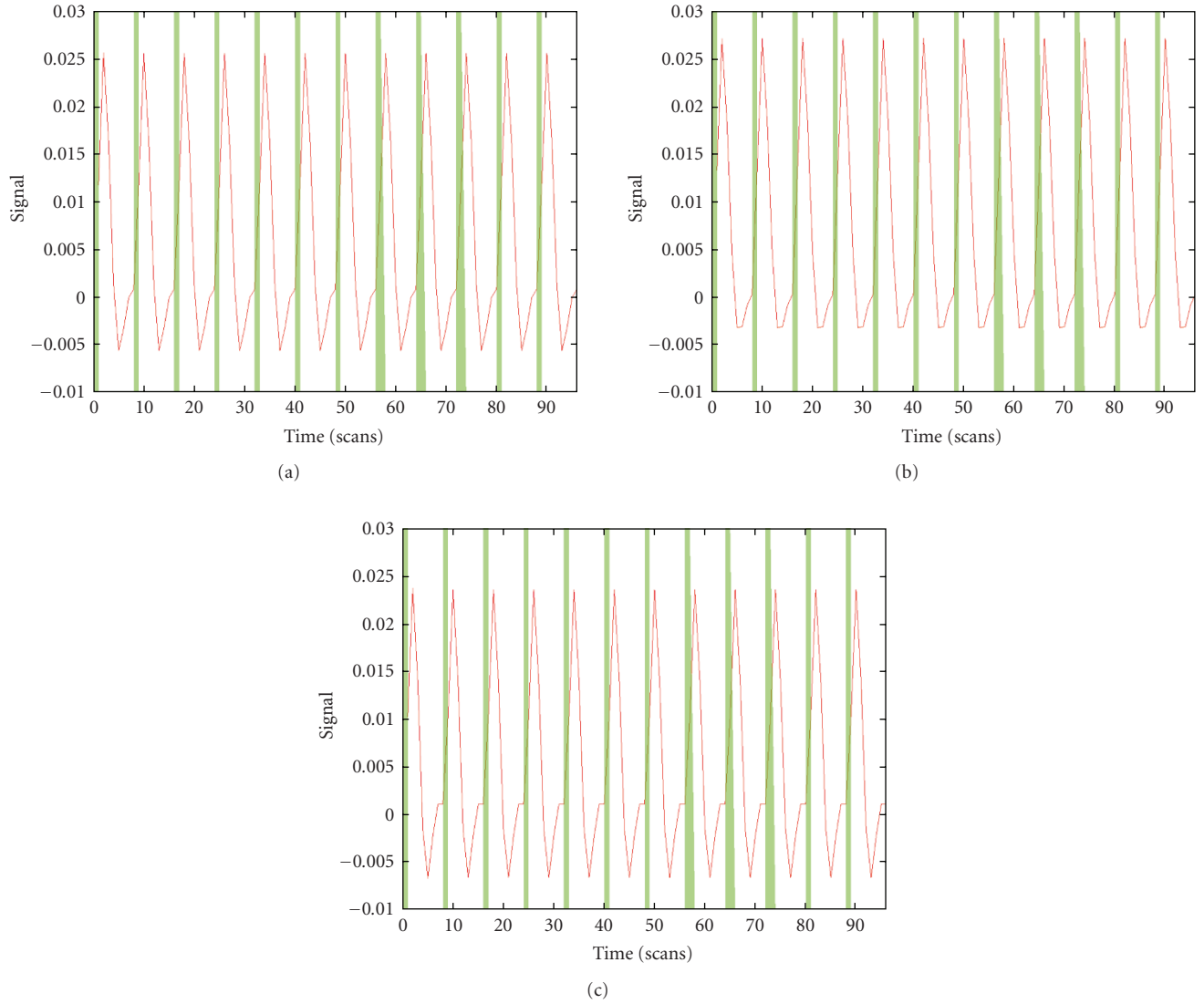

Figure 3: Simulated Datasets with three parameter sets. Each stimulus event, which was simulated by rectangular pulse of width 2-seconds.

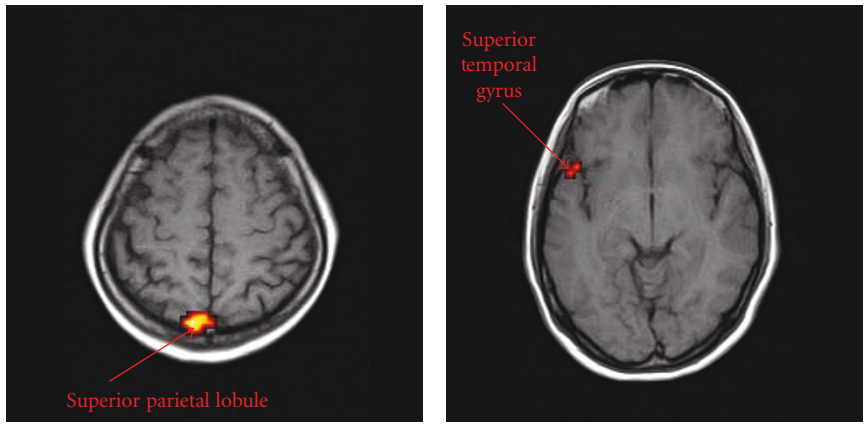

Figure 4: The activation map for the texture perception experiment. The red arrowheads indicate the location of ROI, which is the most strongly activated voxel in their own activation blobs.

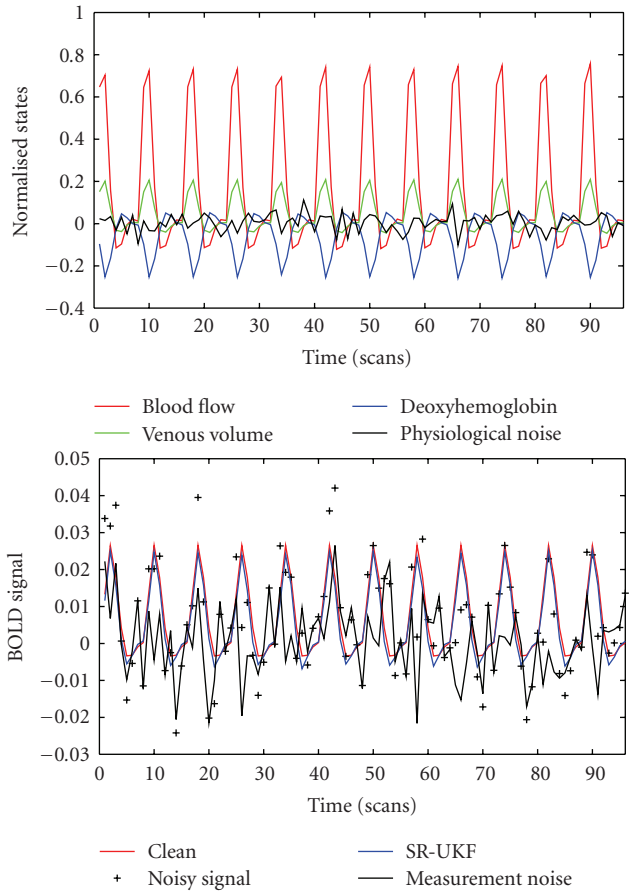

Figure 5: Reconstructed blood oxygen level-dependent (BOLD) signal from estimated states.

having the initial values:

$$\begin{aligned}\hat{\mathbf{x}}_0 &= \mathbb{E}[\mathbf{x}_0],\\ \mathbf{S}_0 &= \text{chol}\left\{\mathbb{E}\left[(\mathbf{x}_0-\hat{\mathbf{x}}_0)(\mathbf{x}_0-\hat{\mathbf{x}}_0)^T\right]\right\},\\ \mathbf{S}_v &= \sqrt{\mathbf{R}_v},\\ \mathbf{S}_w &= \sqrt{\mathbf{R}_w},\end{aligned} \tag{11}$$

where α determines the size of the sigma-point distribution, and is usually set to $1e-4 \le \alpha \le 1$, β is a constant, equal to 2 for a Gaussian distribution, L is the states dimension, $\lambda = L(\alpha^2-1)$ and $\eta = \sqrt{(L+\lambda)}$ is scaling parameter, and $\{W_i\}$ is a set of scalar weights ($W_0^{(m)} = \lambda/(L+\lambda)$, $W_0^{(c)} = \lambda/(L+\lambda) + (1-\alpha^2+\beta)$, $W_i^{(m)} = W_i^{(c)} = 1/\{2(L+\lambda)\}$, $i = 1,\ldots,2L$). $\mathbf{R_v}$ is the process-noise covariance, $\mathbf{R_w}$ is the observation-noise covariance, and $\mathbf{A} \pm \mathbf{u}$ indicates the linear algebra operation of adding a column vector $\mathbf{u}$ to each column of the matrix $\mathbf{A}$. $\text{qr}\{\cdot\}$ is the QR decomposition of a matrix, chol is calculating the matrix square root of the state covariance via a Cholesky factorization, and cholupdate is Cholesky factor updating (available in Matlab as cholupdate).

In our case, both the system state $\mathbf{x}_k$ and the set of model parameters β for the dynamic system must be simultaneously

Table 2: The final values of the parameter estimates for the simulated data. $\alpha = 0.33$ and $V_0 = 0.02$ are assumed known.

Region	ϵ	τ_s	τ_f	τ_0	E_0
Set 1	0.54	1.54	2.46	0.98	0.34
Set 2	0.59	1.38	2.7	0.89	0.3
Set 3	0.49	1.7	2.22	1.07	0.4

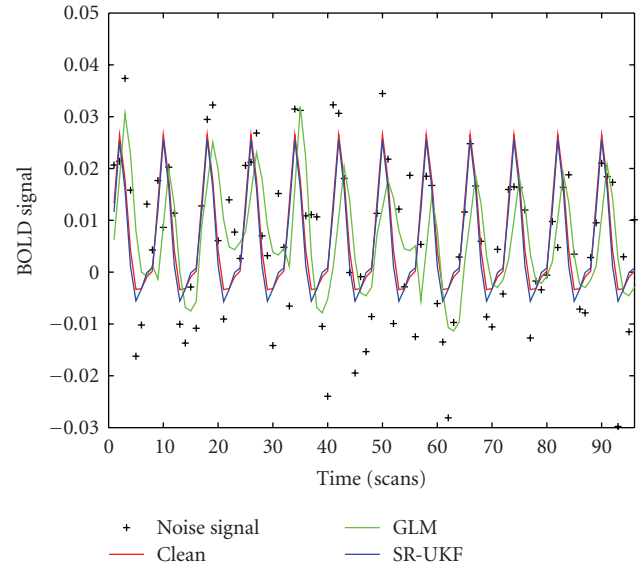

Figure 6: Comparison between the BOLD signal estimates obtained with the general linear model (GLM) and Balloon model.

estimated from only the observed noisy signal $\mathbf{y}_k$. In the joint filtering approach, the unknown system state and parameters are concatenated into a single higher-dimensional joint state vector, $\tilde{\mathbf{x}}_k$, that is,

$$\tilde{\mathbf{x}}_k = \left[\mathbf{x}^T \quad \boldsymbol{\beta}^T\right]^T, \tag{12}$$

and the state space model is reformulated as

$$\begin{aligned}\tilde{\mathbf{x}}_{k+1} &= \tilde{\mathbf{f}}(\tilde{\mathbf{x}}_k, \mathbf{u}_k, \tilde{\mathbf{v}}_k),\\ \mathbf{y}_k &= \tilde{\mathbf{h}}_k(\tilde{\mathbf{x}}_k, \mathbf{w}_k),\end{aligned} \tag{13}$$

which can be expanded to

$$\begin{aligned}\begin{bmatrix}\mathbf{x}_{k+1}\\ \boldsymbol{\beta}_{k+1}\end{bmatrix} &= \begin{bmatrix}\mathbf{f}\left(\mathbf{x}_k, \mathbf{u}_k, \mathbf{v}_k; \boldsymbol{\beta}_k\right)\\ \boldsymbol{\beta}_k\end{bmatrix} + \begin{bmatrix}0\\ \mathbf{r}_k\end{bmatrix},\\ \mathbf{y}_k &= \mathbf{h}\left(\mathbf{x}_k, \boldsymbol{\beta}_k, \mathbf{w}_k\right),\end{aligned} \tag{14}$$

where $\tilde{\mathbf{x}}_k = [\mathbf{w}_k^T \; \mathbf{r}_k^T]^T$. A single SR-UKF is now run on the augmented state space, that is joint state vector $\tilde{\mathbf{x}} = \{\dot{f}, f, v, q, \epsilon, \tau_s, \tau_f, \tau_0, E_0\}^T$ in here, to produce simultaneous estimates of the states $\mathbf{x}_k$ and the parameters β.

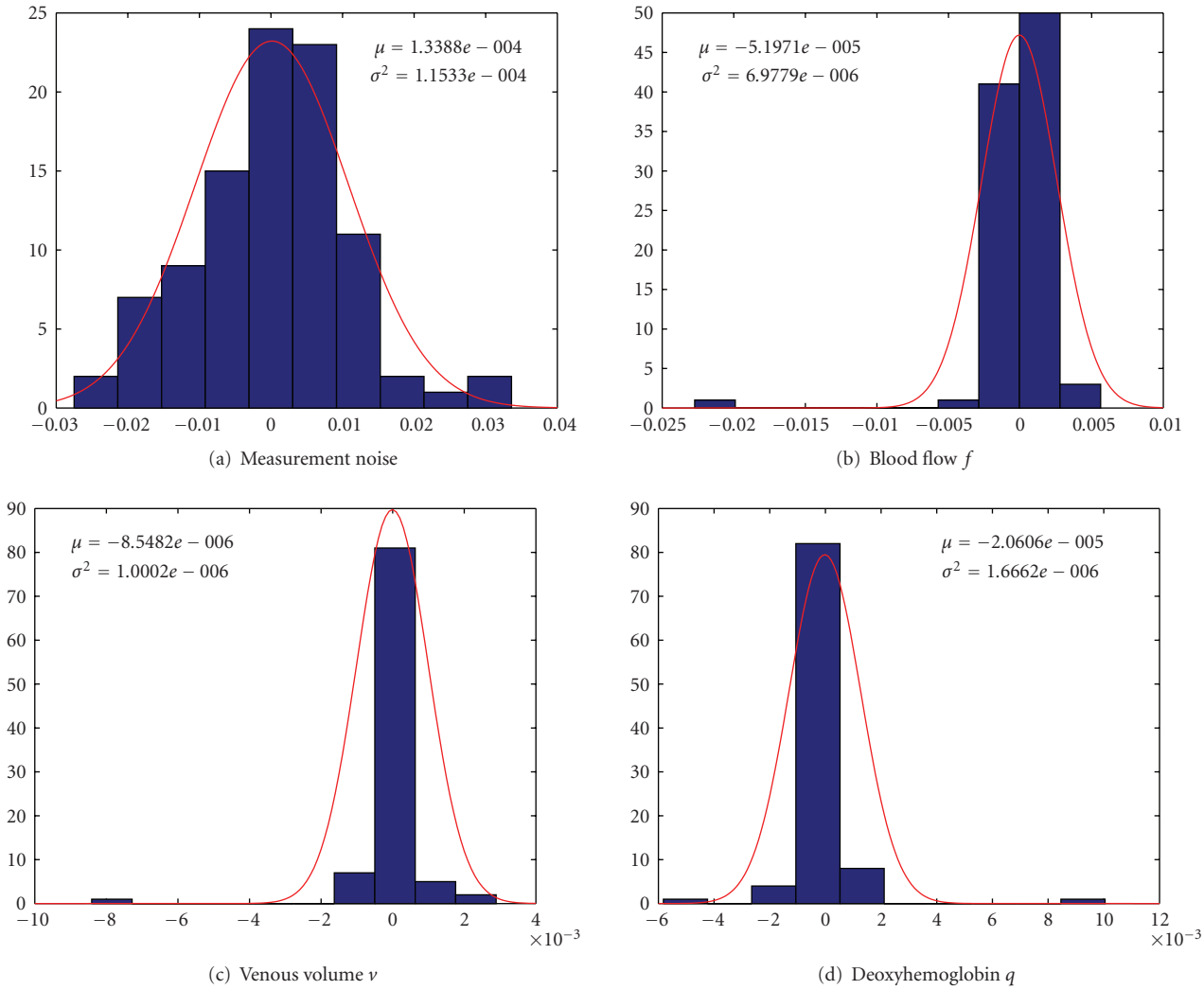

(a) Measurement noise (b) Blood flow f

(c) Venous volume v (d) Deoxyhemoglobin q

FIGURE 7: The histogram of estimated measurement and physiological noise from synthetic data. The red line represents fitted Gaussian function.

Since the differential equations in (3) are not soluble analytically, we employ a fourth-order Runge-Kutta method to investigate the information about the trajectory, where step length h was set as 0.2-second to make the truncation error involved sufficiently small. In other words, we used a Runge-Kutta scheme to approximate $\mathbf{F}(\mathbf{x}_k, \mathbf{u}_k)$ and $\mathbf{H}(\mathbf{x}_k)$, given $\mathbf{F}(\mathbf{x}_k, \mathbf{u}_k)$ and $\mathbf{H}(\mathbf{x}_k)$ in (4). Furthermore, while the initial input $u_0 = 1$, the states necessarily converge to their equilibrium points $\mathbf{x}_0 = [0, \epsilon\tau_f + 1, (\epsilon\tau_f + 1)^{\alpha}, ((1 - (1 - E_0)^{1/(\epsilon\tau_f + 1)})/E_0)(\epsilon\tau_f + 1)^{\alpha}]^T$ (Section 3), thus the initial condition was set as $\tilde{\mathbf{x}}(0) = [0, 2.328, 1.322, 0.635, 0.54, 1.54, 2.46, 0.98, 0.34]^T$.

5. Experimental Results

5.1. Simulated Data. Since the ground truth is unavailable in a real fMRI data, simulated data are chosen to examine the filtering estimation algorithm. We design three artificial BOLD responses, with three distinct sets of values for the parameters (Figure 3). The system parameters are set in their typical ranges (Table 2). The experimental condition of synthetic dataset is consistent with a real fMRI experiment (Section 5.2), including external neuronal input $u(t)$ and scan numbers. Then we add onto these BOLD responses the white Gaussian noise with intensities proportional to the spectral power of noise-free time courses.

For each simulated time courses, the data assimilation is performed. Our unscented Kalman filter treats the states and parameters as unknown quantities and estimates their posterior densities, given observed data. This is referred to as a dual estimation scheme. It relies upon knowing the covariance or precision (inverse covariance) of the state noise, $\mathbf{R}_v$, the observation noise, $\mathbf{R}_w$, and the Kalman gain, $\mathcal{K}$. In our simulations, we assumed that the data assimilation scheme had access to the true and known values of these covariances and used sensible values for our analysis of the real fMRI time series. The initial prior parameters were set to within 10% of their true value used in assimilations. Figure 5 shows a representation of

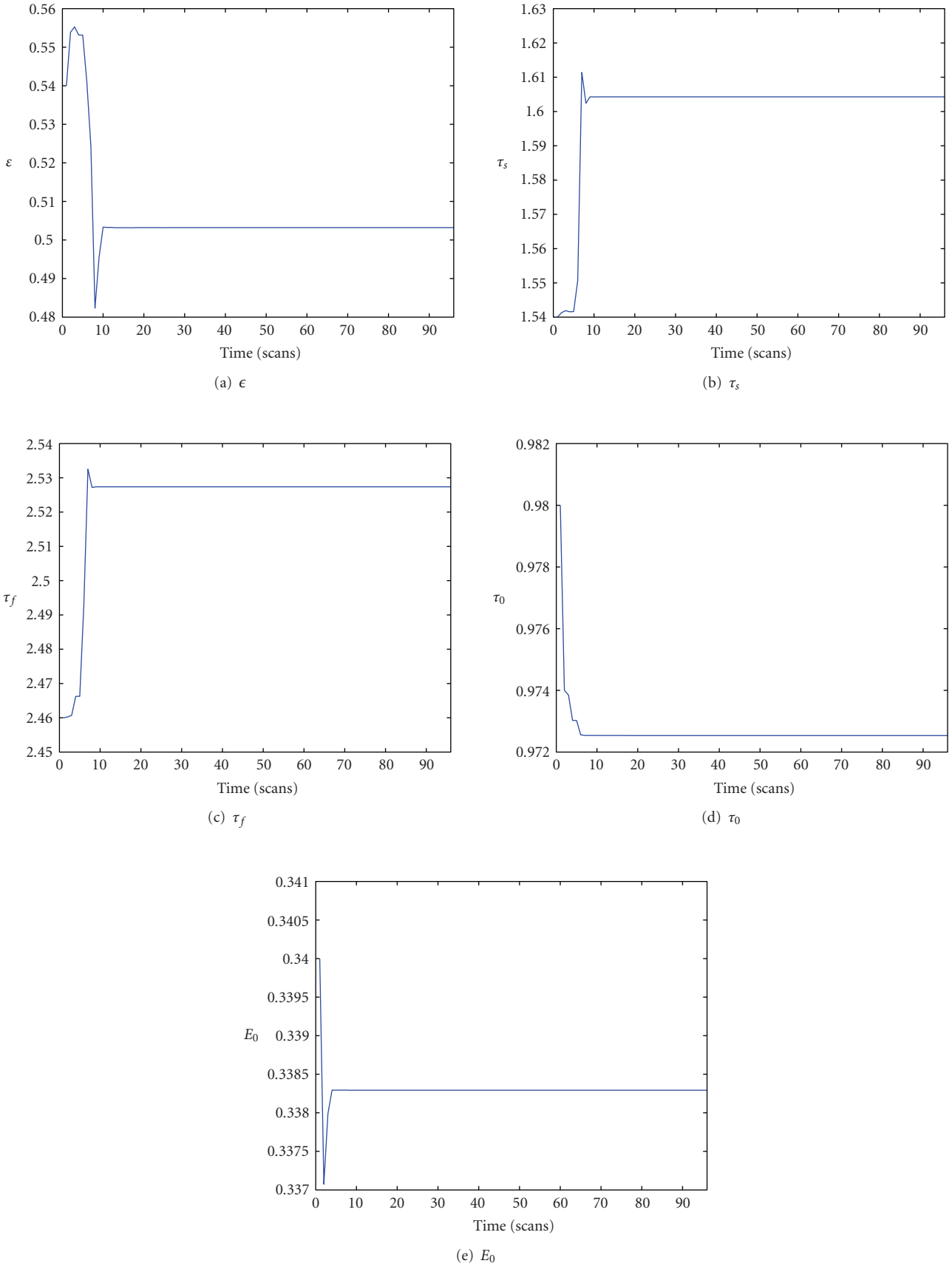

Figure 8: Convergence of parameter estimates.

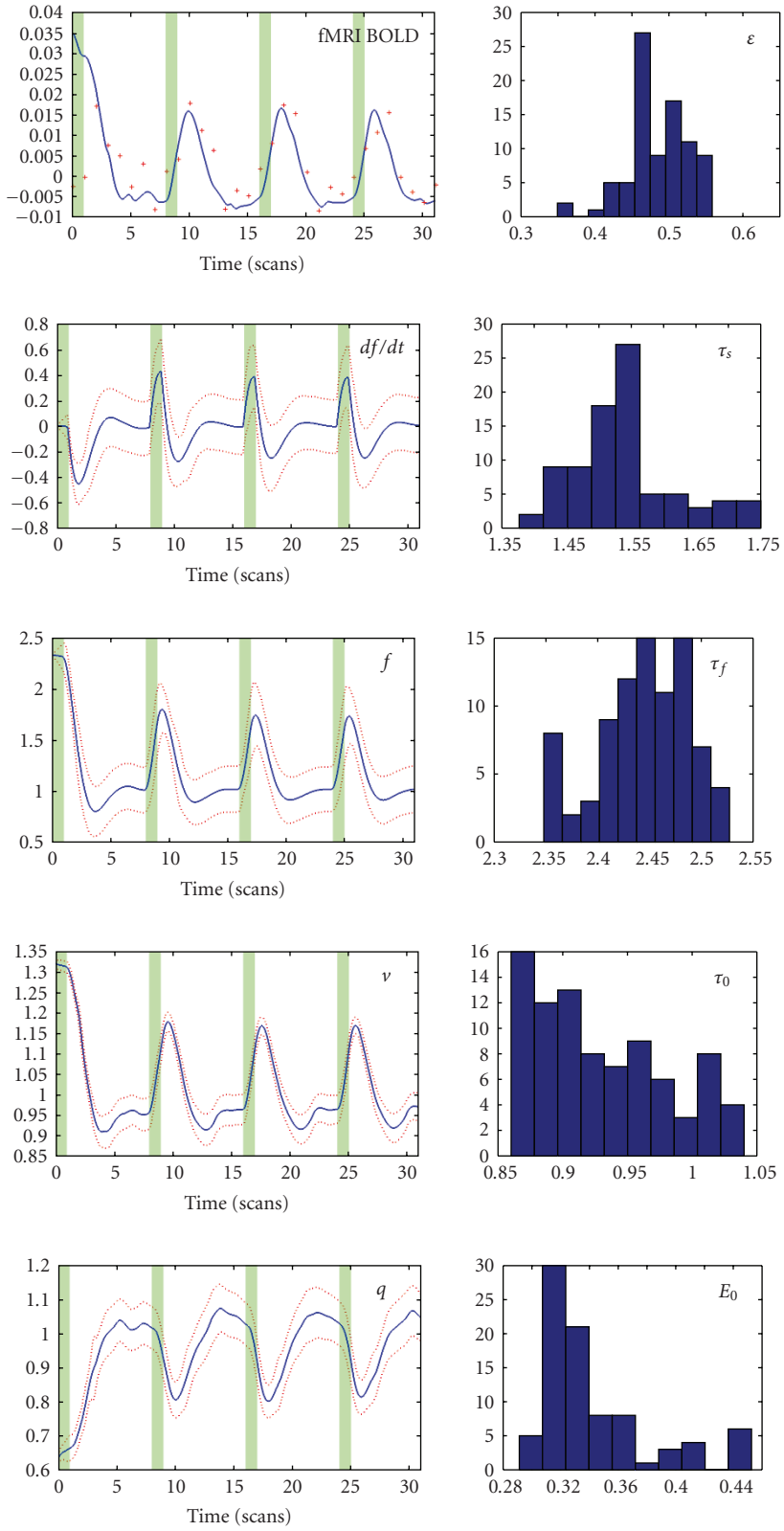

Figure 9: The left column shows time series of the estimated states functions of hemodynamic response to touch perception tasks. From top to bottom: BOLD signal y (the measured signal (red plus sign) and the filtering process (blue line)), $\dot{f}$, f, v, and q. Note that our inversion scheme allows for random fluctuations on the parameters. This means that we have distribution as opposed to a point estimate for these quantities. These distributions are shown in the right column. From top to bottom: ϵ, τ_s, τ_f,τ_0, E_0. Each stimulus event, which was simulated by rectangular pulse of width 2-seconds, is shown as strips in green. These red bounds are given by its standard deviation σ.

Table 3: The expectations over time of the parameter estimates from ROIs with the presented nonlinear filtering algorithm.

	ϵ	τ_s	τ_f	τ_0	E_0
LPs	0.5985	1.4953	2.4889	1.0871	0.5272
GTs	0.2761	1.5421	2.4616	0.9400	0.5120

the reconstructed hemodynamic state trajectories (top) and the estimated BOLD signal (bottom) generated by SR-UKF (CNR = 1). Both physiological noise and measurement noise were presented as black line. Our approach produced better BOLD signal estimates than a traditional GLM approach (Figure 6). Furthermore, the histograms for the random errors of the estimated BOLD signal and each physiological states are also plotted in Figure 7. The red line represents the fitted Gaussian function. The estimated means μ and variance σ^2 for the Gaussian distribution are also shown in Figure 7. The results clearly show that physiological noise and measurement noise are normally distributed with mean zero, consistent with our assumptions about the probabilistic distribution of the random error. Each parameter estimate converged within the 10 iterations, as shown in Figure 8.

5.2. Human Data. The volunteering participant was a healthy, right-handed, male graduate student (age 27), claiming to be in good health with no history of neurological or psychological illness. The participant was instructed on the tasks prior to scanning and was provided with a brief practice period.

Two distinct texture photographs were presented in 2-seconds for touch perception followed by a 14-seconds rest. Scanning was synchronized with the onset of the first stimulate. In total, 96 acquisitions were made (RT = 2-seconds), in periods of 16*s*, giving 1216-second circles. Functional images were acquired on a 1.5-Tesla scanner (Marconi EDGE ECLIPSE) using a standard fMRI gradient echo echo-planar imaging (EPI) protocol (TE, 40 ms; TR, 2500 ms; flip angle, 90°; NEX, 1; FOV, 24 cm; resolution, 64 × 64 matrix). Sixteen contiguous 6-mm-thick, 0.5-mm-intervals were acquired to provide a coverage of the entire brain.

The initial eight scans were discarded to avoid magnetic saturation effects. The remaining images were realigned and corrected for movement-related effects within SPM (Wellcome Department of Cognitive Neurology, http://www.fil.ion.ucl.ac.uk/spm). All volumes were rescaled to the same global mean to focus on regional changes. The data were then subject to the activation detection of hierarchic statistical inference methods for the nonlinear models. The stimulus input function $u(t)$, the supposed neuronal activity, was simply given as a square wave. The resulting map, testing for activation due to texture perception, was thresholded at $P = .05$ (corrected) [19]. Two regions of interest in the right superior parietal lobule and the left superior temporal gyrus that showed the largest response to stimulations in their own blobs were selected for analysis (see Figure 4).

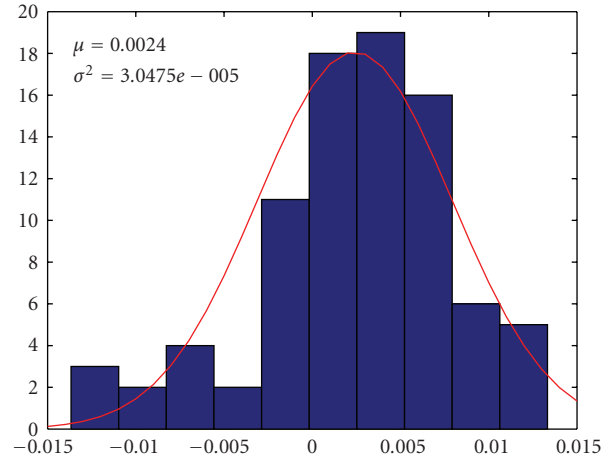

Figure 10: The histogram of estimated measurement noise. The red line represents fitted Gaussian function.

For two regions of interest, we identified all four states and five parameters of the nonlinear hemodynamic model by the technique mentioned above. The system noise is assumed as $\mathbf{R}_v = 0.01E(9)$, and the measurement noise is assumed as $\mathbf{R}_w = 0.005$. Figure 9 shows subsegments of the estimated behavior of the state functions and system parameters of the hemodynamic approach for the superior parietal lobule. Each stimulus event, which was simulated by rectangular pulse of width 2-seconds, is shown as strips in green. The column on the right shows the histogram of the estimated parameters. The left column shows the time series of the estimated state functions of the hemodynamic response to touch perception tasks. The final value of the Kalman gain estimates is $\mathcal{K} = [0.0647, 0.15, 0.2368, -1.035, 0.3458, 0.0659, 0.1698, 0.4356, -0.0554]^T$. Furthermore, the histogram of the estimated system parameters is shown in the right column. The values of these parameters are all in the range of previous reports [10, 13]. These physiological plausible parameters estimated in voxels may provide valuable information to evaluate activation. Figure 10 shows the histogram of estimated measurement noise. The fitted Gaussian function is also plotted as a red line. Table 3 lists the estimated parameters of the hemodynamic model from ROI with the presented filtering algorithm. All parameter estimates fall within a standard deviation of the expectation value reported by previous studies.

6. Conclusion

In this paper, we describe a way of assimilating fMRI time series that allow one to make inferences about the underlying physiological states and the biophysical parameters generating observed fMRI signals. This corresponds to a nonlinear deconvolution of observed data using a hemodynamic state-space model based on stochastic differential equations. It allows one to deconvolve data, given known experimental inputs or perturbations. Our model can be regarded as a stochastic Dynamic Causal Model for a signal brain

region, which allows for noise or random fluctuations on the underlying or hidden physiological states. Our deconvolution scheme uses an unscented Kalman filter and, computationally, is equivalent to the complexity of linear deconvolution schemes. In addition to inferring the hidden states we also provide for inference on the parameters. This involves augmenting the state vector with the parameters and treating them as slowly varying states (as in variable parameter regression and related approaches).

In conclusion, we presented a nonlinear filtering approach, which deals with the nonlinear propagation of the probability density function (pdf) in a straight, deterministic sample points way, for hemodynamic data assimilation. This approach results in approximations of the posterior mean and covariance in at least the second order (Taylor series expansion), depending on different sampling strategy, with equivalent computational expense to existing linearization filtering algorithm. Hence, it can raise the potential of the hemodynamic model for more accurate inferences about the parameters of the model, given the data. However, although, these benefits have been achieved, there are shortcomings in this approach. The neuroimaging community had been concerned predominantly with the functional localization. The statistic strategy for activation detection that is appropriate to the filtering approach still needs more work.

Acknowledgments

This work is supported by the National Natural Science Foundation of China (nos: 30570538, 30770615, 30800250), Zhejiang Provincial Natural Science Foundation of China (no: Y2080281), and Doctoral Fund of Ministry of Education of China (no: 200803351022).

References

[1] K. J. Friston, A. P. Holmes, K. J. Worsley, J. B. Poline, C. R. Williams, and R. S. J. Frackowiak, "Analysis of functional MRI time-series," *Human Brain Mapping*, vol. 1, pp. 153–171, 1994.

[2] J. C. Rajapakse, F. Kruggel, J. M. Maisog, and D. Y. von Cramon, "Modeling hemodynamic response for analysis of functional MRI time-series," *Human Brain Mapping*, vol. 6, no. 4, pp. 283–300, 1998.

[3] K. J. Friston, P. Fletcher, O. Josephs, A. P. Holmes, M. D. Rugg, and R. Turner, "Event-related fMRI: characterising differential responses," *NeuroImage*, vol. 7, pp. 30–40, 1998.

[4] P. Ciuciu, J.-B. Poline, G. Marrelec, J. Idier, C. Pallier, and H. Benali, "Unsupervised robust nonparametric estimation of the hemodynamic response function for any fMRI experiment," *IEEE Transactions on Medical Imaging*, vol. 22, no. 10, pp. 1235–1251, 2003.

[5] M. Lindquist and T. Wager, "Modeling the hemodynamic response function using inverse logit functions," in *Proceedings of Human Brain Mapping Annual Meeting*, 2005.

[6] G. H. Glover, "Deconvolution of impulse response in event-related BOLD fMRI," *NeuroImage*, vol. 9, no. 4, pp. 416–429, 1999.

[7] P. L. Purdon, V. Solo, R. M. Weisskoff, and E. N. Brown, "Locally regularized spatiotemporal modeling and model comparison for functional MRI," *NeuroImage*, vol. 14, no. 4, pp. 912–923, 2001.

[8] T. Obata, T. T. Liu, K. L. Miller, W.-M. Luh, E. C. Wong, L. R. Frank, and R. B. Buxton, "Discrepancies between BOLD and flow dynamics in primary and supplementary motor areas: application of the balloon model to the interpretation of BOLD transients," *NeuroImage*, vol. 21, no. 1, pp. 144–153, 2004.

[9] R. B. Buxton, E. C. Wong, and L. R. Frank, "Dynamics of blood flow and oxygenation changes during brain activation: the balloon model," *Magnetic Resonance in Medicine*, vol. 39, no. 6, pp. 855–864, 1998.

[10] K. J. Friston, A. Mechelli, R. Turner, and C. J. Price, "Nonlinear responses in fMRI: the balloon model, volterra kernels, and other hemodynamics," *NeuroImage*, vol. 12, no. 4, pp. 466–477, 2000.

[11] K. J. Friston, "Bayesian estimation of dynamical systems: an application to fMRI," *NeuroImage*, vol. 16, no. 2, pp. 513–530, 2002.

[12] T. Deneux and O. Faugeras, "Using nonlinear models in fMRI data analysis: model selection and activation detection," *NeuroImage*, vol. 32, no. 4, pp. 1669–1689, 2006.

[13] J. J. Riera, J. Watanabe, I. Kazuki, et al., "A state-space model of the hemodynamic approach: nonlinear filtering of BOLD signals," *NeuroImage*, vol. 21, no. 2, pp. 547–567, 2004.

[14] L. A. Johnston, E. Duff, and G. F. Egan, "Partical filtering for nonlinear BOLD signal analysis," in *Proceedings of the 9th International Conference on Medical Image Computing and Computer-Assisted Intervention (MICCAI '06)*, pp. 292–299, Copenhagen, Denmark, October 2006.

[15] L. A. Johnston, E. Duff, I. Mareels, and G. F. Egan, "Nonlinear estimation of the BOLD signal," *NeuroImage*, vol. 40, no. 2, pp. 504–514, 2008.

[16] M. S. Arulampalam, S. Maskell, N. Gordon, and T. Clapp, "A tutorial on particle filters for online nonlinear/non-Gaussian Bayesian tracking," *IEEE Transactions on Signal Processing*, vol. 50, no. 2, pp. 174–188, 2002.

[17] K. J. Friston, N. Trujillo-Barreto, and J. Daunizeau, "DEM: a variational treatment of dynamic systems," *NeuroImage*, vol. 41, no. 3, pp. 849–885, 2008.

[18] K. J. Friston, "Variational filtering," *NeuroImage*, vol. 41, no. 3, pp. 747–766, 2008.

[19] Z. H. Hu and P. C. Shi, "Nonlinear anaysis of BOLD signal: biophysical modeling, physiological states, and functional activation," in *Proceedings of the International Conference on Medical Image Computing and Computer-Assisted Intervention (MICCAI '07)*, pp. 734–741, 2007.

[20] Y. Zheng, J. Martindale, D. Johnston, M. Jones, J. Berwick, and J. Mayhew, "A model of the hemodynamic response and oxygen delivery to brain," *NeuroImage*, vol. 16, no. 3, part 1, pp. 617–637, 2002.

[21] R. B. Buxton, K. Uludağ, D. J. Dubowitz, and T. T. Liu, "Modeling the hemodynamic response to brain activation," *NeuroImage*, vol. 23, supplement 1, pp. S220–S233, 2004.

[22] Y. Zheng, D. Johnston, J. Berwick, D. Chen, S. Billings, and J. Mayhew, "A three-compartment model of the hemodynamic response and oxygen delivery to brain," *NeuroImage*, vol. 28, no. 4, pp. 925–939, 2005.

[23] Z. H. Hu and P. C. Shi, "Sensitivity analysis for biomedical model," *processing*.

[24] S. J. Julier and J. K. Uhlmann, "Reduced sigma point filters for the propagation of means and covariances through nonlinear transformations," in *Proceedings of the American Control Conference (ACC '02)*, pp. 887–892, Anchorage, Alaska, USA, May 2002.

[25] S. J. Julier and J. K. Uhlmann, "Unscented filtering and nonlinear estimation," *Proceedings of the IEEE*, vol. 92, no. 3, pp. 401–422, 2004.

[26] R. van der Merwe and E. A. Wan, "The square-root unscented Kalman filter for state and parameter-estimation," in *Proceedings of the IEEE International Conference on Acoustics, Speech and Signal Processing (ICASSP '01)*, vol. 6, pp. 3461–3464, Salt Lake, Utah, USA, May 2001.